Hydrol. Earth Syst. Sci. Discuss., 9, 11999–12028, 2012
www.hydrol-earth-syst-sci-discuss.net/9/11999/2012/
doi:10.5194/hessd-9-11999-2012

Hydrology and Earth System Sciences Discussions

On-line multistep-ahead inundation depth forecasts by recurrent NARX networks

H.-Y. Shen and L.-C. Chang

Department of Water Resources and Environmental Engineering, Tamkang University, Tamsui, Taiwan

Received: 22 September 2012 – Accepted: 10 October 2012 – Published: 22 October 2012

Correspondence to: L.-C. Chang (changlc@mail.tku.edu.tw)

Published by Copernicus Publications on behalf of the European Geosciences Union.

Abstract

Various types of artificial neural networks (ANNs) have been successfully applied in hydrological fields, but relatively scant on flood inundation forecast. This study proposes a recurrent configuration of nonlinear autoregressive with exogenous inputs (NARX) network, called R-NARX, to forecast multistep-ahead inundation depths in an inundation area. The proposed R-NARX is constructed based on the recurrent neural network (RNN), which is commonly used for modeling nonlinear dynamical systems. The models were trained and tested based on a large number of inundation data generated by a well validated two-dimensional simulation model at thirteen inundation-prone sites in Yilan County, Taiwan. We demonstrate that the R-NARX model can effectively inhibit error growth and accumulation when being applied to on-line multistep-ahead inundation forecasts over a long lasting forecast period. For comparison, a feedforward time-delay and an on-line feedback configuration of NARX networks (T-NARX and O-NARX) were performed. The results show that (1) T-NARX networks cannot make on-line forecasts due to unavailable inputs in the constructed networks even though they provide the best performances for reference only; and (2) R-NARX networks consistently outperform O-NARX networks and can be adequately applied to on-line multistep-ahead forecasts of inundation depths in the study area during typhoon events.

1 Introduction

The increasing frequency and severity of floods caused by climate change and/or land overuse has been continuously reported both nationally and globally, especially in Southeast Asia, in the last two decades. Taiwan is located in the Northwestern Pacific Ocean, where the activities of subtropical jet streams are frequent. Typhoon Morakot struck Southern Taiwan with a sudden rainfall (the highest rainfall reaching 1166 mm day^{-1}) on 8 August 2009, and the extreme rainfall induced vast mudslides and disastrous flooding throughout Southern Taiwan. A mudslide buried the whole Xiaolin

Village, which caused an estimated 500 deaths. In brief, Typhoon Morakot resulted in 665 deaths, 34 missing, numerous refugees, and roughly NT$ 110 billion (US$ 3.3 billion) in damages. In 2010, Typhoons Fanapi and Megi hit Southern and Eastern Taiwan in mid-September and mid-October, respectively. Both typhoons resulted in loss of life and property, and severely damaged city functions. Flood depth forecasting is an important component of the contingency plan for alleviating flood risk and loss of life and property.

Flooding in urban areas poses a great challenge to hydrologists because of the complex interactions and disruptions associated with non-riverine urban flooding. In the past few decades, simulations of flood inundation extent have been made by the advances in numerical modeling techniques (Bates et al., 1995; Lane, 1998; Marks and Bates, 2000; Bates and De Roo, 2000; Hsu et al., 2000; Wheater, 2002; Kang, 2009) and the use of SAR (synthetic aperture radar) (Bates et al., 2006; Mason et al., 2007; Zwenzner and Voigt, 2009). Conventional inundation models could provide regional hydro-geologic characteristics in response to various patterns of storm events (Hsu et al., 2000; Bates et al., 2003), which are useful information to flood management in early and/or planning stages, nevertheless these models commonly require substantial computational time for iterative solutions to simulate high-resolution spatial flood depths. Consequently, on-line inundation forecasts could not be effectively conducted by conventional inundation models. The great potentiality of artificial neural networks in hydrological time series forecasting and their encouraging results obtained in literature were many (i.e. Maier and Dandy, 2000; Brath et al., 2002; Toth and Brath, 2007; Chen and Chang, 2009; Abrahart et al., 2012). The majority of the applications are river flow forecasting, nevertheless, there are relatively few researches on on-line flood inundation applications. Valeriano et al. (2009) stated that inundation areas were estimated using topographic characteristics based on the simulated overflow volumes recorded at the control point downstream. Chang et al. (2010) integrated artificial neural networks (ANNs) with K-means clustering method, called clustering-based hybrid inundation model (CHIM), to forecast 1-h-ahead inundation extents and depths.

HESSD
9, 11999–12028, 2012

Leedal et al. (2010) proposed 2-D real-time probabilistic inundation maps based on a modified Kalman filter model coupled into 2-D hydrodynamic model to compute the maximum multistep-ahead inundation extent. Pan et al. (2011) used hybrid ANNs in rainfall-inundation forecasting to estimate 1-h-ahead inundation depths.

Because of extremely limited response time to flood disasters in urban areas of Taiwan, reliable multistep-ahead inundation depth forecasts would be helpful in managing contingencies and emergencies and in alleviating flood risk and loss of life and property. However, on-line multistep-ahead flood depth forecasts face two challenges. The first challenge involves extending one-step-ahead forecasting to multistep-ahead forecasting. In one-step-ahead forecasting tasks, ANN models estimate the next sample value without feeding back its output to the model's input layer. In other words, the input contains only observed values. For multistep-ahead forecasting tasks, current inputs would be repeatedly mapped onto various multistep-ahead outputs, or model outputs would be sequentially fed back to the input layer to provide one-step further forecasts. In the latter case, the input layer might contain not only observed values but also model outputs. As known, feeding model outputs back to the input layer makes the model become a dynamic modeling task, which is substantially more complex than static modeling tasks. For these complex tasks, recurrent neural networks (RNNs) play an important role (Menezes Jr. and Barreto, 2008; Chang et al., 2012). RNNs usually incorporate with the architecture of a multilayer perceptron (MLP) for an exploitation of its nonlinear mapping capability (Haykin, 2009). For instance, the simple recurrent network (Elman, 1990) has the outputs of the hidden layer been fed back to the input layer, and demonstrates its great ability in extracting dynamic time variation characteristics. In recent years, RNNs have been applied to the field of hydrological modeling (Chang et al., 2002, 2004; Coulibaly et al., 2005; Besaw et al., 2010; Chiang et al., 2010).

The other challenge is the lack of real-time observed inundation depths, and thus models usually require proceeding with on-line forecasts through the whole period of a typhoon event (commonly over 20 h in our cases) without any observed flood depths. As known, a small prediction error at the beginning can accumulate and propagate in the future (Parlos et al., 2000), which results in poor prediction accuracy when models keep on making forecasts for a long time. To solve the lack of observed depths and mitigate error propagation in the long-run, this study proposes a recurrent configuration for a nonlinear autoregressive with exogenous inputs (NARX) network, called R-NARX, to construct multistep-ahead inundation depth forecast models. To verify its practicability, the Yilan County in Northern Taiwan is used as the study area and another two types (i.e. time-delay and on-line configurations) of NARX networks are also implemented for fully exploring their capabilities in multistep-ahead flood inundation forecasts.

2 NARX network

NARX is an important and useful mathematical model of discrete-time nonlinear systems. Nonlinear systems can be approximated by an MLP network, called NARX, a powerful dynamic model for time series prediction (Jiang and Song, 2011; Menezes Jr. and Barreto, 2008). The architecture of an NARX network based on a multilayer perceptron neural network consists of p antecedent values of exogenous input vectors $\boldsymbol{X}(t)$, such as on-line rainfall intensity; q antecedent actual values $z(t+n-q)$, such as inundation depths, which are tapped-delay inputs or fed back from the model's output; and a single output $\hat{z}(t+n)$. For many practical applications in hydrological systems, such as flood inundation depth forecasting in this study, we commonly face the problem of lacking on-line data. ANNs are well known data-driven models. In case of no on-line data available, we have to find a way to train and test the networks step-by-step in real time through the whole flooding period. Bearing this in mind as a motivation, we propose three configurations of the NARX network to fully explore and examine their capabilities of learning and generalization in flood inundation depth forecast tasks.

HESSD
9, 11999–12028, 2012

2.1 Learning algorithms

Three types of configured NARX networks are: (1) time-delay-based static network (T-NARX); (2) on-line feedback T-NARX network (O-NARX); and (3) recurrent-based network (R-NARX).

In the T-NARX network (Fig. 1), all the inputs (p antecedent rainfalls and q antecedent inundation depths) are observed values in both training and testing phases. The T-NARX network is indeed a feedforward time-delay neural network (TDNN), which is a static neural network and frequently used to predict theoretical time series with long-range dependence present in data. *The proper synaptic weights of the network can be obtained using the batch mode of the standard back-propagation learning algorithm for searching minimum errors during the training phase*. The constructed network and its synaptic weights would be fixed in the testing phase. In reality, only real-time rainfall values could be obtained, while real-time observed inundation depths could not be obtained on-line. Moreover, when inundation depth forecasts are conducted for more than two-h-ahead ($n > 1$), the q antecedent actual values ($z(t+n-1)$, $z(t+n-2), \ldots, z(t+n-q)$) are future data and cannot be obtained at present time. Consequently, the constructed T-NARX could not conduct on-line forecasting. The T-NARX network is implemented mainly to find the optimal solution, where the long-range dependences inside the input-output patterns could be extracted and the solution could be provided as a reference.

It is interesting to learn the reliability (training data set) and generalization (testing data set) of the models constructed above. Alternatively, we propose the O-NARX to investigate the capability of T-NARX networks constructed in the case of no on-line q antecedent actual inundation depths available. After the networks have been constructed, the model outputs of inundation depths ($\hat{z}(t)$) are fed back to the input layer for on-line forecasting in both training and testing phases (Fig. 2). It is noted that the O-NARX networks are exactly the same as the T-NARX networks except for two major differences: the q antecedent actual inundations of the T-NARX models; and the model

HESSD
9, 11999–12028, 2012

outputs fed back to the input layer in both training and testing phases of the O-NARX models for on-line multistep-ahead forecasting.

We intended to further solve the problem of no actual values during the on-line process and propose to use the model outputs of inundation depths as the inputs in both training and testing phases. In this way, the NARX networks would be trained with imperfect information as well as remaining similar characteristics of input-output patterns in the training and testing phases, and therefore we argued the configured NARX networks would maintain similar capability of on-line multistep-ahead forecasts in both phases. Figure 3 shows that, at time $t+n$, *the previous model output is fed back to the input layer through a delay-line memory of* q *units*. The synaptic weights of the network can be adjusted using the *on-line back-propagation learning algorithm* to search for minimum errors on *an example-by-example basis during the training phase and eventually reach a stable condition, where the error could not be further deduced and all the synaptic weights then remain the same in the following search process*. The constructed network and its synaptic weights *would be fixed in the testing phase to evaluate its applicability and reliability in new events (input-output patterns)*. We notice that the input information based on model outputs is not perfect (real) which could include different fault levels. It is interesting to learn how well the configured networks can perform by learning imperfect inputs. That is to examine the effect of inhibition ability of the constructed networks on error growth and accumulation.

2.2 Mathematical formulation

This study minimizes the energy function by the steepest descent method, and the recurrent configuration is used to adjust the synaptic weights on an example-by-example basis. The mathematical formulation of the R-NARX is presented as follows.

The network contains M exogenous inputs and a single output. For simplicity, assume that $p=0$, $q=1$, and $n=1$ in Fig. 3. Let $\boldsymbol{x(t)}$ denote the $M \times 1$ input vector, $\hat{z}(t+1)$ denote the corresponding single output, and $\boldsymbol{y(t+1)}$ denote the corresponding $N \times 1$ output vector in the hidden layer. The input $\boldsymbol{x(t)}$ and one-step delayed output $\hat{z}(t)$

HESSD
9, 11999–12028, 2012

are concatenated to form the $(M+1)\times 1$ vector $\boldsymbol{\mu(t)}$, of which the ith element is denoted by $\mu_i(t)$. Let A denote the set of indices i, for which $x_i(t)$ is an external input, and B denote the set of indices i, for which $\hat{z}(t)$ is the output of the network. We thus have

$$\mu_i(t) = \begin{cases} x_i(t) \text{ if } & i \in A \\ \hat{z}(t) \text{ if } & i \in B \end{cases} \tag{1}$$

Let $\mathbf{W}$ denote the $N \times (M+1)$ weight matrix of the hidden layer. Let $\mathbf{V}$ denote the $N \times 1$ weight matrix of the output layer. The net activity of neuron j at time t is computed by

$$\text{net}_j(t+1) = \sum_{i \in A \cup B} w_{ji}\mu_i(t) \tag{2}$$

The output of neuron j is obtained by passing $\text{net}_j(t+1)$ through the nonlinearity $f(.)$, yielding

$$y_j(t+1) = f(\text{net}_j(t+1)) \tag{3}$$

The net output in the output layer at time t is computed by

$$\text{net}(t+1) = \sum v_j y_j(t+1) \tag{4}$$

$$\hat{z}(t+1) = f(\text{net}(t+1)) \tag{5}$$

Let $z(t+1)$ denote the target value at time $t+1$. The error $e(t+1)$ is given as,

$$e(t+1) = z(t+1) - \hat{z}(t+1) \tag{6}$$

Define the *instantaneous value* of the network error at time $t+1$ as the energy function.

$$E(t+1) = \frac{1}{2}e^2(t+1) \tag{7}$$

HESSD
9, 11999–12028, 2012

H.-Y. Shen and L.-C. Chang

For the sequential model of the back-propagation learning algorithm, the negative gradient ($-\nabla E$) of the energy function is used to adjust the synaptic weights at each time step. The weight change for any particular weight v_j can thus be written as

$$\Delta v_j = -\eta_1 \frac{\partial E(t+1)}{\partial v_j} \tag{8}$$

where η_1 is the learning-rate parameter.

Consequently,

$$\frac{\partial E(t+1)}{\partial v_j} = -e(t+1)\frac{\partial \hat{z}(t+1)}{\partial v_j} = -e(t+1)f'(\text{net}(t+1))\left(y_j(t+1) + \sum_j v_j \frac{\partial y_j(t+1)}{\partial v_j}\right) \tag{9}$$

$$\frac{\partial y_j(t+1)}{\partial v_j} = f'(\text{net}_j(t+1))w_{ji}\frac{\partial \hat{z}(t)}{\partial v_j} \tag{10}$$

$$\frac{\partial \hat{z}(t+1)}{\partial v_j} = f'(\text{net}(t+1))\left[y_j(t+1) + \sum_j v_j \left(f'(\text{net}_j(t+1))w_{ji}\frac{\partial \hat{z}(t)}{\partial v_j}\right)\right] \tag{11}$$

The same method is also implemented for weight w_{ji}, where $\Delta w_{ji} = -\eta_2 \frac{\partial E(t+1)}{\partial w_{ji}}$, and η_2 is the learning-rate parameter. The partial derivative $\frac{\partial E(t+1)}{\partial w_{ji}}$ can be obtained by the chain rule for differentiation, shown as follows:

$$\frac{\partial E(t+1)}{\partial w_{ji}} = -e(t+1)\frac{\partial \hat{z}(t+1)}{\partial w_{ji}} = -e(t+1)f'(\text{net}(t+1))\sum_j v_j \frac{\partial y_j(t+1)}{\partial w_{ji}} \tag{12}$$

$$\frac{\partial y_j(t+1)}{\partial w_{ji}} = f'(\text{net}_j(t+1))\left[u_i(t) + w_{ji}\frac{\partial \hat{z}_i(t)}{\partial w_{ji}}\right] \tag{13}$$

HESSD
9, 11999–12028, 2012

$$\frac{\partial \hat{z}(t+1)}{\partial w_{ji}} = f'(\mathrm{net}(t+1)) \left[\sum_j v_j f'(\mathrm{net}_j(t+1)) \left(u_i + w_{ji} \frac{\partial \hat{z}(t)}{\partial w_{ji}} \right) \right] \tag{14}$$

As compared with the learning algorithm of TDNN, we would like to note that the proposed algorithm has an additional term in both Eqs. (11) and (14), in which $\hat{z}(t)$ is a function of w_{ji} (or v_j), while in TDNN $z(t)$ is not a function of w_{ji} (or v_j) but an observation value.

3 Study area and materials

Yilan County is selected as the case study. It is the most beautiful urban county near Taipei City, but it has a long history of flooding problems, which continue threatening the lives and livelihoods of its residents. Yilan County, located in Northeastern Taiwan, spans an area of approximately 2143 km^2 and is divided by three river basins (Toucheng, Lanyoung and Nan'ao). In the last two decades, Yilan has frequently suffered from flood disasters that resulted in grave losses of agricultural crops and private property. Thirteen villages have been identified as inundation-prone sites by the government project on the renovation of inundation-prone areas. The thirteen inundation-prone sites are used to investigate the robustness and stability of the proposed models in this study. Figure 4 shows the thirteen inundation-prone sites and three nearby rain gauges.

Because historical observed data of inundation depths are rare and no historical hydrogpaph of inundation depths is available for storm events, we have to find other data sets to build forecast models. Fortunately, the synthetic hydrographs of flood depths were obtained from the Water Resources Agency (WRA), Taiwan, which were well validated by the urban inundation model linkage of the HEC-1 model, SWMM (the storm water management model) and the two-dimensional non-inertial overland flow simulation model. The urban inundation model proposed by Hsu et al. (2000) was

HESSD
9, 11999–12028, 2012

implemented to simulate inundation in urban areas, where the movement of water in the studied area is characterized by the sewer flow component and the surcharge-induced inundation component. SWMM is employed to provide the surcharged flow hydrographs for surface runoff exceeding the capacity of the storm sewers and the 2-D diffusive overland-flow model considering the non-inertia equation with alternative direction explicit numerical scheme was used to calculate the detailed inundation zones and depths due to the surcharged water on overland surface. The detail description of the urban inundation models (including SWMM and 2-D diffusive overland-flow model) and its application for a 100-yr 24-h design rainfall of analyzing surface inundation in the Taipei city can be found in Hsu et al. (2000).

There were 24 design rainfall events and 31 historical rainfall events. The 24 design rainfall events are comprised by various return periods of three nearby rain gauges. The 24-h design hyetograph pattern of all rain gauges and the cumulative rainfall for various return periods (10-, 25-, 100- and 200-yr) in three nearby rain gauges are shown in Fig. 5 and Table 1, respectively. The 31 historical rainfall events are shown in Table 2. The corresponding *24-h flood inundation depth hydrographs to those events (24 design events and 31 historical events) were obtained from the WRA, Taiwan, and used to configure the models*. The proposed models of thirteen sites in this study area are then thoroughly trained and tested based on flood inundation data generated by the well validated inundation model with the design rainfall patterns and/or historical rainfall events. The maximums, means and variances of flood inundation depths at 13 sites are shown in Table 3. It appears that the maximums, means and variances of the training case are much larger than those of the testing case at all sites. This is mainly because the return periods of 24 design storms (only used in the training case) are much larger than those of historical typhoon events (mainly used in the testing case).

HESSD
9, 11999–12028, 2012

4 Results

This study investigates the multistep-ahead inundation forecast performances of three types of NARX networks based on a large number of rainfall-inundation patterns for all thirteen inundation-prone sites in Yilan County. The performances of these three models are evaluated by the root mean square error (RMSE), as shown below.

$$\mathrm{RMSE} = \sqrt{\frac{\sum_{i=1}^{n} (\hat{H}_i - H_i)^2}{n}} \tag{15}$$

where $\hat{H}_i$ and H_i are the estimated flood depth and the simulated flood depth of the ith data, respectively.

For each inundation-prone site, one- to six-h-ahead ($n = 1$–6) flood depths forecast models are constructed by the T-, O- and R-NARX networks, and there are 624 training data (26 events × 24 h) and 696 testing data (29 events × 24 h). The inputs include current and two previous hourly rainfalls (t, $t-1$ and $t-2$, i.e. $p = 2$ in this study) of three nearby rain gauges and one hour before the nth-hour forecasted flood depth ($t+n-1$, i.e. $q = 1$ in this study), and the output is the next n step ($t+n$) flood depth. The input dimension is 10 and the output dimension is only 1. After implementing an intensive trial-and-error procedure based on the training data set, the networks are constructed to have only one hidden layer with three nodes, which in general would have the most suitable performances for all models of three inundation-prone sites. The networks are then applied to the testing data set without further modifications. The summarized results of the three models are presented in Table 4. It represents the results of one- to six-h-ahead forecasting for the maximum, minimum, and average RMSEs of 13 sites in Yilan County. The maximum (minimum) indicates the maximum (minimum) value occurs at one of the 13 sites, while the mean indicates the average RMSE value of 13 sites. The results show that the RMSEs of T-NARX networks are relatively smaller than

HESSD
9, 11999–12028, 2012

H.-Y. Shen and L.-C. Chang

the other two networks in all cases. These values indicate the optimal results we might reach based on the perfect anticipant conditions (rainfall and inundation depths).

We first examine the results of T-NARX and O-NARX, which have exactly the same structures and synaptic weights at each site. Apparently, T-NARX models have much better performances, in terms of much smaller RMSE values, than O-NARX models for all the cases in both training and testing cases, especially in the testing cases. These results provide clear and rigid evidences that the reliability and generalization of the constructed networks are poor in the training data set and bad in the testing data set if on-line antecedent inundation depths could not be obtained, which indeed is the common situation we have.

As we compared the results of O-NARX and R-NARX, the RMSEs of the O-NARX are much larger than that of the R-NARX in all cases. For instance, the mean RMSEs of six-hour-ahead forecast in the testing cases are 0.36 m and 0.24 m for O-NARX and R-NARX models, respectively; and the maximum RMSEs of six-h-ahead forecast in the training cases are 0.34 m and 0.23 m for O-NARX and R-NARX models, respectively. These results indicate that R-NARX networks provide much better (accurate and reliable) forecasts than O-NARX networks.

Figure 6 shows the RMSE growth trends of one- to six-hour-ahead forecasts of three models in the training and testing data sets. For one- to six-hour-ahead flood depth forecasts, the RMSEs of T-NARX, R-NARX and O-NARX models increase slightly, moderately and dramatically, respectively, in both phases. Again, the T-NARX has the best performances (the smallest RMSEs) among three models; whereas R-NARX models have better performances than O-NARX models, especially in the testing data set.

To illustrate the forecasting accuracy of O-NARX and R-NARX models, the scatter plots of the simulated versus forecasted flood depths of site 2 (one-, three- and six-hour-ahead) in the testing data sets are shown in Fig. 7, respectively. In the R-NARX model, almost all pairs of forecasted and simulated points scatter closely to the diagonal line for flood depths in Fig. 7. In the O-NARX model, only one- and

HESSD
9, 11999–12028, 2012

three-hour-ahead flood depths scatter suitably around the diagonal line. According to the results, the R-NARX provides a significantly superior performance to the O-NARX.

Figure 8 shows the growth trends of the mean RMSE at 13 sites for one- to six-hour-ahead forecasts of R-NARX and O-NARX models through on-line forecasts proceeding from the 1st hour to the 24th hour in the testing phase. It is noticed that the model outputs would gradually apart from true values as the forecasting proceeds, and feeding those imperfect outputs back to the input layer would further accelerate the growth of forecast errors. The mean RMSE growth trends of R-NARX models increase gradually, whereas those of O-NARX models increase rapidly. This demonstrates that the R-NARX model has substantially smaller error accumulation and propagation than the O-NARX model, and the proposed R-NARX networks can provide reasonable and robust results for multistep-ahead flood depth forecasts if real-time observed rainfall and the feedback of model inundation outputs to the input layer can be implemented as the forecasting proceeds.

5 Conclusions

Due to the lack of observed inundation depths in on-line situations, modeling multistep-ahead inundation depth forecast is a challenging task. This paper presents a recurrent configuration for nonlinear autoregressive with exogenous inputs network (R-NARX) to build on-line multistep-ahead inundation depth forecasts based on the model outputs of inundation depth as the input. To compare and verify the reliability of the R-NARX model, the time delay-based network (T-NARX) and on-line configured network (O-NARX) were also applied to thirteen inundation-prone sites in Yilan County, Taiwan, using a great number of design storms and historical typhoons rainfall-inundation patterns synthesized from a well validated simulation model to train and test the configured networks. The three models were built to perform one- to six-hour-ahead inundation forecasting, and the on-line forecast lasting for 24 h. The results show the findings: (1) given perfect input information in both training and testing phases, the

HESSD
9, 11999–12028, 2012

T-NARX networks could offer the most accurate flood depth forecasts than the other two networks, nevertheless in case of only imperfect input information available, the O-NARX networks, which have exactly the same structures and synaptic weights as the T-NARX networks, would provide the worst forecast performances in all the cases; (2) the R-NARX model can indeed capture the trends of flood depth hydrographs suitably for multistep-ahead forecasting because it can use imperfect input information to train the network; (3) the on-line multistep-ahead forecasting by the R-NARX model can continuously proceed for a long period (24 h in this study case) only based on rainfall information and the feedback of model's forecasting output and thus maintain acceptable accuracy; and (4) the RMSE improvement rates of the R-NARX model are high than 30 % in all one- to six-h-ahead on-line forecasts as compared with the O-NARX model.

The results demonstrate that the R-NARX model has the ability to tolerate imperfect inputs and mitigate error accumulation and propagation effectively when forecasting over a long period. The R-NARX network has an outstanding capability for multistep-ahead forecasting on flood depths and can on-line proceed for a long period.

Acknowledgements. The authors gratefully acknowledge the financial support for this research by the Water Resources Agency, Ministry of Economic Affair, Taiwan, R.O.C. (Grant No. MOEAWRA1000101). Simulated data provided by the Hydrotech Research Institute, National Taiwan University, are greatly appreciated.

References

Abrahart, R. J., Anctil, F., Coulibaly, P., Dawson, C. W., Mount, N. J., See, L. M., Shamseldin, A. Y., Solomatine, D. P., Toth, E., and Wilby, R. L.: Two decades of anarchy? Emerging themes and outstanding challenges for neural network river forecasting, Prog. Phys. Geog., 36, 480–513, 2012.

Bates, P. D. and De Roo, A. P. J.: A simple raster-based model for flood inundation simulation, J. Hydrol., 236, 54–77, 2000.

Bates, P. D., Anderson, M. G., and Hervouet, J. M.: Initial comparison of 2-dimensional finite-element codes for river flood simulation, P. I. Civil. Eng.-Water, 112, 238–248, 1995.

Bates, P. D., Marks, K. J., and Horritt, M. S.: Optimal use of high-resolution topographic data in flood inundation models, Hydrol. Process., 17, 537–557, doi:10.1002/hyp.1113, 2003.

Bates, P. D., Wilson, M. D., Horritt, M. S., Mason, D. C., Holden, N., and Currie, A.: Reach scale floodplain inundation dynamics observed using airborne synthetic aperture radar imagery: data analysis and modelling, J. Hydrol., 328, 306–318, 2006.

Besaw, L. E., Rizzo, D. M., Bierman, P. R., and Hackett, W. R.: Advances in ungauged stream-flow prediction using artificial neural networks, J. Hydrol., 386, 27–37, 2010.

Brath, A., Montanari, A., and Toth, E.: Neural networks and non-parametric methods for improving real-time flood forecasting through conceptual hydrological models, Hydrol. Earth Syst. Sci., 6, 627–639, doi:10.5194/hess-6-627-2002, 2002.

Chang, F. J., Chang, L. C., and Huang, H. L.: Real-time recurrent learning neural network for stream-flow forecasting, Hydrol. Process., 16, 2577–2588, 2002.

Chang, L. C., Chang F. J., and Chiang Y. M.: A two-step-ahead recurrent neural network for stream-flow forecasting, Hydrol. Process., 18, 81–92, 2004.

Chang, L. C., Shen, H. Y., Wang, Y. F., Huang, J. Y., and Lin, Y. S.: Clustering based hybrid inundation model for forecasting flood inundation depths, J. Hydrol., 385, 257–268, 2010.

Chang, L. C., Chen, P. A., and Chang, F. J.: Reinforced two-step-ahead weight adjustment technique for online training of recurrent neural networks, IEEE T. Neural Networ., 23, 1269–1278, 2012.

Chen, Y. H. and Chang, F. J.: Evolutionary artificial neural networks for hydrological systems forecasting, J. Hydrol., 367, 125–137, 2009.

Coulibaly, P. and Baldwin, C. K.: Nonstationary hydrological time series forecasting using nonlinear dynamic methods, J. Hydrol., 307, 164–174, 2005.

Elman, J. L.: Finding structure in time, Cognitive Sci., 14, 179–211, 1990.

Haykin, S.: Neural networks and learning machines, 3rd Edn., Pearson Prentice Hall, New Jersey, 2009.

Jiang, C. and Song, F.: Sunspot forecasting by using chaotic time-series analysis and NARX network, JCP, 6, 1424–1429, 2011.

Kang, S. H.: The application of integrated urban inundation model in Republic of Korea, Hydrol. Process., 23, 1642–1649, 2009.
Lane, S. N.: Hydraulic modelling in hydrology and geomorphology: a review of high resolution approaches, Hydrol. Process., 12, 1131–1150, 1998.
Leedal, D, Neal, J., Beven, P., Young P., and Bates P.: Visualization approaches for communicating real-time forecasting level and inundation information, J. Flood Risk Manag., 3, 140–150, 2010.
Maier, H. R. and Dandy, G. C.: Neural networks for the prediction and forecasting of water resources variables: a review of modeling issues and applications, Environ. Modell. Softw., 15, 101–104, 2000.
Marks, K. and Bates, P.: Integration of high-resolution topographic data with floodplain flow models, Hydrol. Process., 14, 2109–2122, 2000.
Mason, D. C., Horritt, M. S., Dall'Amico, J. T., Scott, T. R., and Bates, P. D.: Improving river flood extent delineation from synthetic aperture radar using airborne laser altimetry, IEEE T. Geosci. Remote, 45, 3932–3943, 2007.
Menezes Jr., J. M. P. and Barreto, G. A.: Long-term time series prediction with the NARX network: an empirical evaluation, Neurocomputing, 71, 3335–3343, 2008.
Pan, T.-Y., Lai, J.-S., Chang, T.-J., Chang, H.-K., Chang, K.-C., and Tan, Y.-C.: Hybrid neural networks in rainfall-inundation forecasting based on a synthetic potential inundation database, Nat. Hazards Earth Syst. Sci., 11, 771–787, doi:10.5194/nhess-11-771-2011, 2011.
Parlos, A. G., Rais, O. T., and Atiya, A. F.: Multi-step-ahead prediction using dynamic recurrent neural networks, Neural Networks, 13, 765–786, 2000.
Toth, E. and Brath, A.: Multistep ahead streamflow forecasting: role of calibration data in conceptual and neural network modeling, Water Resour. Res., 43, W11405, doi:10.1029/2006WR005383, 2007.
Valeriano, O. C. S., Koike, T., Dawen, Y., Cho, T., Van Khanh, D., and Nguyen, L.: Flood simulation using different sources of rainfall in the Huong River, Vietnam, Hydrolog. Sci. J., 54, 909–917, 2009.
Wheater, H. S.: Progress in and prospects for fluvial flood modelling, Phil. Trans. R. Soc. Lond. A, 360, 1409–1431, 2002.

Yen-Ming Chiang, Li-Chiu Chang, Meng-Jung Tsai, Yi-Fung Wang, and Fi-John Chang: Dynamic neural networks for real-time water level predictions of sewerage systems-covering gauged and ungauged sites, Hydrol. Earth Syst. Sci., 14, 1309–1319, doi:10.5194/hess-14-1309-2010, 2010.

Zwenzner, H. and Voigt, S.: Improved estimation of flood parameters by combining space based SAR data with very high resolution digital elevation data, Hydrol. Earth Syst. Sci., 13, 567–576, doi:10.5194/hess-13-567-2009, 2009.

HESSD

9, 11999–12028, 2012

H.-Y. Shen and L.-C. Chang

Table 1. 24-h cumulative rainfall of design rainfall events at three rainfall gauges.

	24-h cumulative rainfall of design events (mm) Return Period (yr)			
Rain Gauge	10	25	100	200
R1	477.7	576.1	721.9	794.2
R2	364.7	439.0	548.9	603.4
R3	501.3	605.7	764.1	844.7

* All 24 design events were used for training data set.

HESSD
9, 11999–12028, 2012

Table 2. Rainfall information of the 31 historical rainfall events.

event	date	peak of total rainfall intensity ($mm\,h^{-1}$)	peak time (hour)	24-h cumulative rainfall (mm)		
				R1	R2	R3
Typhoon Maggie	5 Jun 1999	92.5	02	186.5	172.5	277.5
Typhoon Kai-Tak	8 Jul 2000	45.5	10	56.1	68.6	89.0
Typhoon Bilis	21 Aug 2000	38.5	01	54.0	43.5	74.0
Storm 01*	29 Oct 2000	28.0	07	46.1	31.6	0.1
Storm 02*	3 Nov 2000	93.5	08	218.5	194.5	187.5
Storm 03	11 Nov 2000	53.5	11	72.5	70.5	154.5
Storm 04	13 Dec 2000	62.0	16	131.5	147.5	164.0
Storm 05	19 Dec 2000	40.0	24	132.1	27.6	120.0
Typhoon Cimaron	11 May 2001	63.5	14	133.0	150.0	134.0
Storm 06	23 Sep 2001	11.5	24	80.0	18.5	23.0
Typhoon Lekima	24 Sep 2001	77.0	07	102.6	144.0	327.0
Typhoon Haiyan	15 Oct 2001	16.5	02	22.5	10.6	10.1
Storm 07	8 Dec 2001	28.0	20	147.1	41.1	27.1
Typhoon Rammasun	2 Jul 2002	58.0	17	53.1	76.6	26.1
Typhoon Vamco	19 Aug 2003	25.5	19	96.5	2.1	55.5
Typhoon Dujuan	31 Aug 2003	71.5	07	136.1	124.5	87.5
Storm 08	10 Sep 2003	27.5	20	41.0	26.5	36.5
Typhoon Conson	7 Jun 2004	105.5	05	110.1	223.5	301.0
Typhoon Aere	23 Aug 2004	3.7	01	0.6	0.6	9.0
Storm 09	7 Sep 2004	51.5	10	24.1	69.1	59.6
Typhoon Nock-Ten	24 Oct 2004	53.5	19	74.1	98.1	68.5
Typhoon Haitang	16 Jul 2005	37.5	02	27.1	53.5	145.5
Typhoon Talim	30 Aug 2005	20.0	01	45.0	57.0	59.5
Typhoon Longwang	30 Sep 2005	28.0	12	91.6	91.6	57.6
Storm 10	9 Jul 2006	65.0	21	330.5	140.0	84.0
Typhoon Shanshan	14 Sep 2006	19.0	24	22.1	32.6	42.6
Typhoon Pabuk	6 Aug 2007	14.5	02	56.0	35.0	20.0
Typhoon Sepat	16 Aug 2007	46.5	13	61.5	58.5	107.0
Storm 11	13 Oct 2007	86.5	24	148.0	114.5	169.5
Storm 12	5 Nov 2007	59.0	14	32.1	32.1	263.6
Storm 13	8 Nov 2007	52.0	10	94.0	83.5	196.5

* Two events are used for training data (*) and the other 29 events are used for testing data.

HESSD
9, 11999–12028, 2012

R-NARX networks for multistep forecasts

H.-Y. Shen and L.-C. Chang

Table 3. Maximum, mean and variance of 13 sites' flood depths.

Spot	Training Max	Mean	Variance	Testing Max	Mean	Variance
S1	2.45	0.87	0.69	1.12	0.24	0.11
S2	3.41	1.44	1.39	1.91	0.36	0.16
S3	3.60	1.53	1.41	1.77	0.37	0.16
S4	2.42	0.89	0.68	1.10	0.24	0.1
S5	2.84	1.18	0.65	1.27	0.36	0.13
S6	1.85	1.13	0.56	1.56	0.41	0.19
S7	3.29	1.24	1.04	1.10	0.32	0.15
S8	2.92	1.22	0.98	1.42	0.32	0.13
S9	3.01	0.99	0.72	1.24	0.28	0.11
S10	2.87	1.35	0.92	1.54	0.39	0.16
S11	2.61	0.89	0.73	1.13	0.24	0.12
S12	2.92	1.25	0.89	1.33	0.32	0.16
S13	3.00	1.27	1.07	1.78	0.35	0.17

HESSD
9, 11999–12028, 2012

HESSD

9, 11999–12028, 2012

R-NARX networks for multistep forecasts

H.-Y. Shen and L.-C. Chang

Table 4. Performance of one- to six-hour-ahead flood depth forecasts of the T-, O- and R-NARX models for all thirteen sites.

RMSE (m)		T-NARX			O-NARX			R-NARX		
		max	min	mean	max	min	mean	max	min	mean
$t+1$	Training	0.10	0.02	0.06	0.17	0.04	0.08	0.13	0.05	0.08
	Testing	0.07	0.03	0.05	0.30	0.07	0.18	0.18	0.06	0.12
$t+2$	Training	0.10	0.02	0.06	0.17	0.04	0.09	0.13	0.05	0.08
	Testing	0.07	0.03	0.05	0.32	0.09	0.19	0.19	0.06	0.13
$t+3$	Training	0.10	0.03	0.06	0.19	0.06	0.11	0.13	0.06	0.09
	Testing	0.08	0.03	0.06	0.34	0.14	0.22	0.24	0.07	0.15
$t+4$	Training	0.11	0.04	0.07	0.21	0.08	0.12	0.14	0.08	0.10
	Testing	0.10	0.04	0.07	0.41	0.15	0.28	0.32	0.10	0.17
$t+5$	Training	0.12	0.04	0.08	0.19	0.10	0.14	0.18	0.07	0.12
	Testing	0.13	0.05	0.09	0.44	0.19	0.33	0.39	0.13	0.21
$t+6$	Training	0.13	0.04	0.09	0.34	0.12	0.19	0.23	0.07	0.14
	Testing	0.15	0.05	0.11	0.50	0.24	0.36	0.40	0.16	0.24

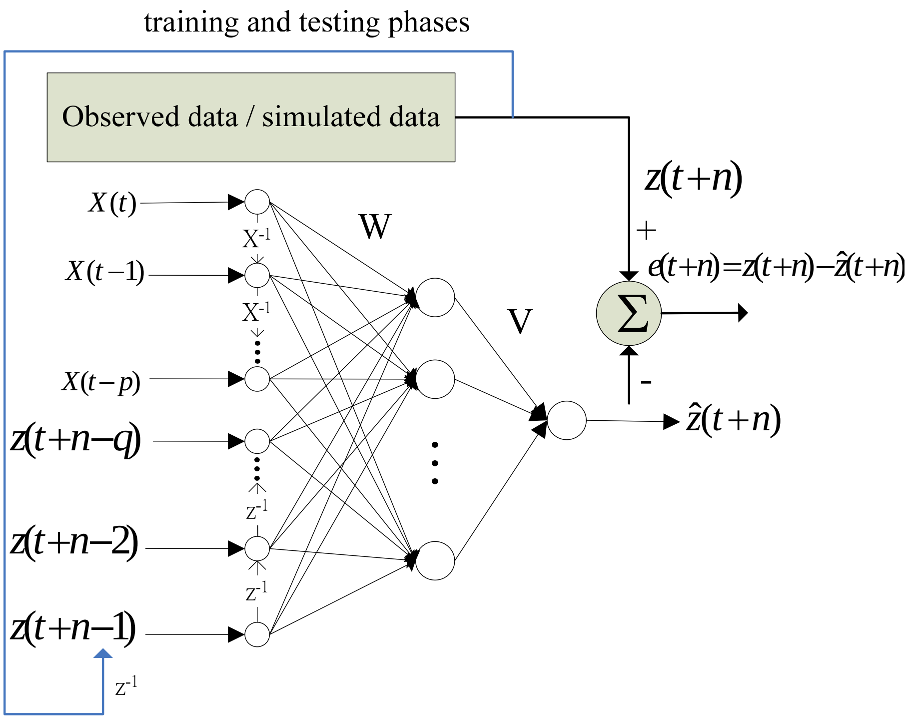

Fig. 1. Architecture of NARX network during training and testing phases in the time delay mode (T-NARX).

HESSD
9, 11999–12028, 2012

Title Page
Abstract | Introduction
Conclusions | References
Tables | Figures
◀| |▶
◀ ▶
Back | Close
Full Screen / Esc
Printer-friendly Version
Interactive Discussion

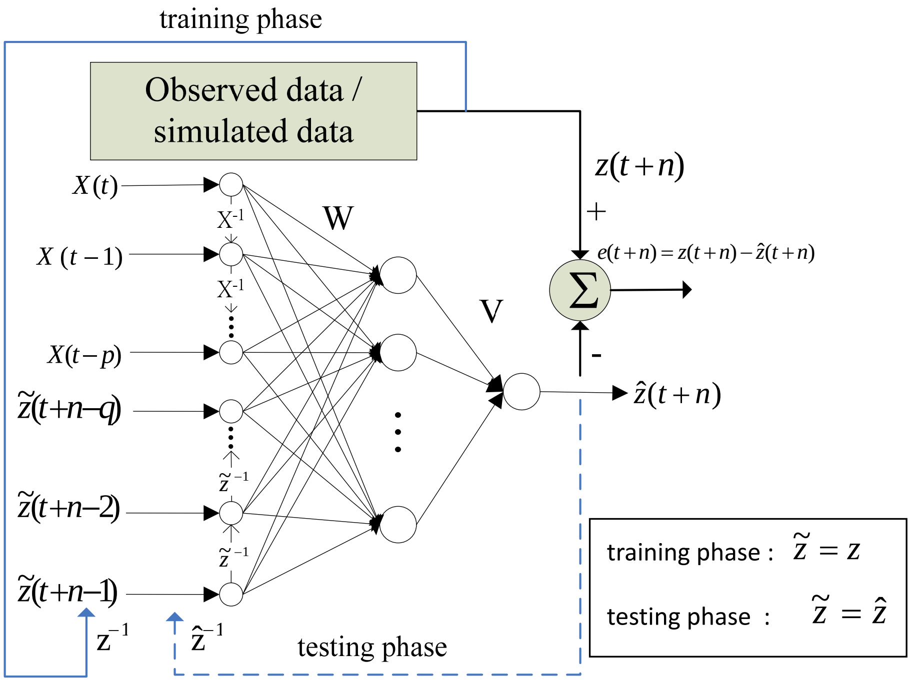

Fig. 2. Architecture of NARX network during training and testing phases in the on-line time delay mode (O-NARX).

HESSD
9, 11999–12028, 2012

R-NARX networks for multistep forecasts

H.-Y. Shen and L.-C. Chang

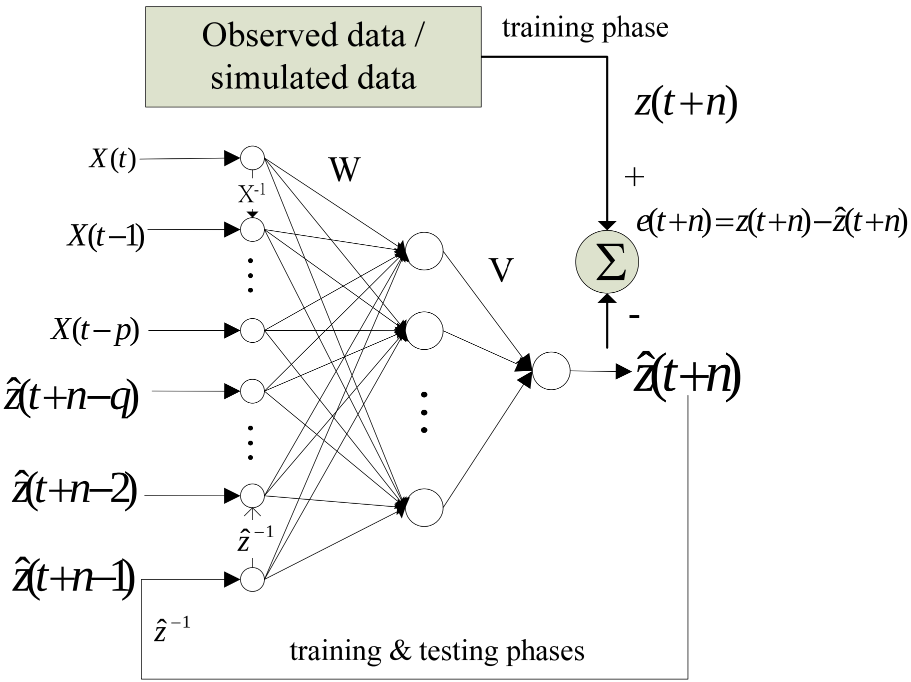

Fig. 3. Architecture of NARX network during training and testing phases in the recurrent mode (R-NARX).

HESSD
9, 11999–12028, 2012

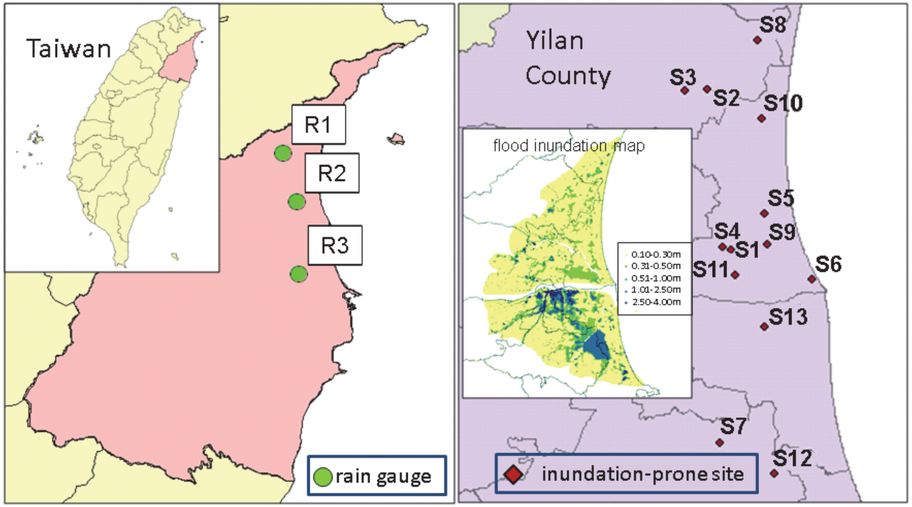

Fig. 4. Locations of Yilan County's inundation-prone sites and nearby rain gauges.

HESSD
9, 11999–12028, 2012

R-NARX networks for multistep forecasts

H.-Y. Shen and L.-C. Chang

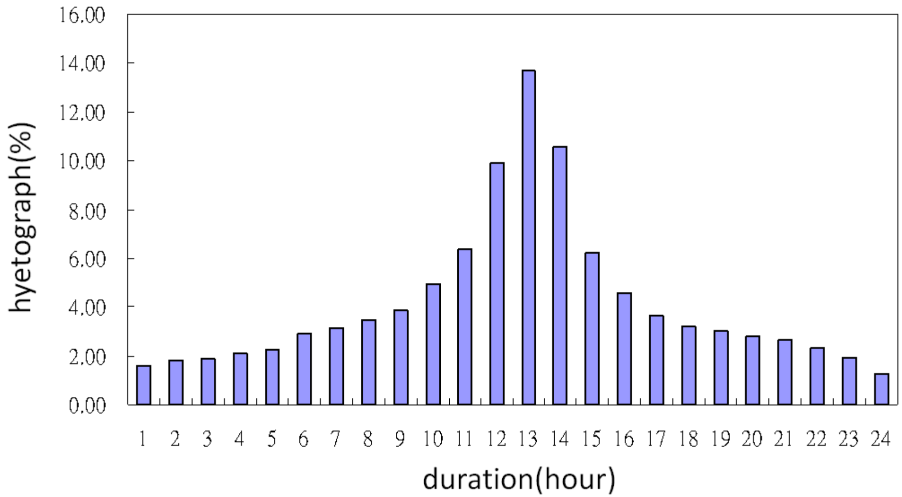

Fig. 5. The 24-h design hyetograph pattern for nearby rain gauges.

HESSD
9, 11999–12028, 2012

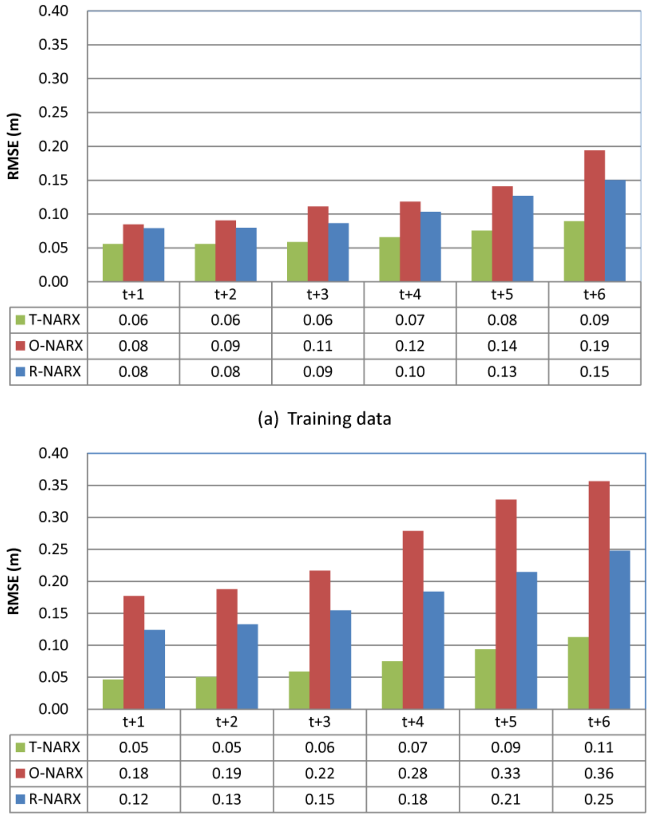

(b)Testing data

Fig. 6. Comparison of T-, O- and R-NARX modes for one- to six-hour-ahead forecasts during training and testing data (the mean RMSE of all sites).

HESSD
9, 11999–12028, 2012

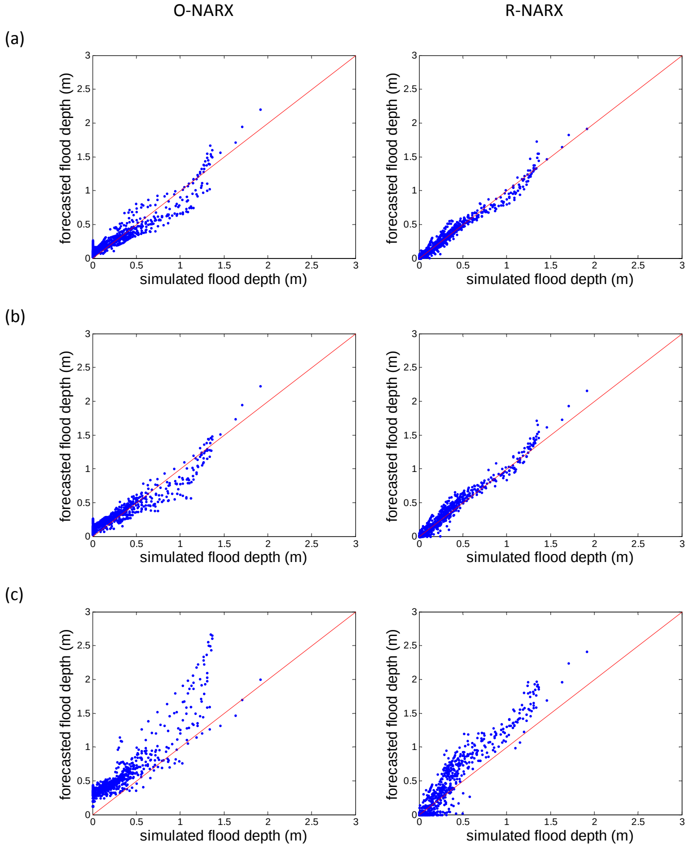

Fig. 7. Comparison of simulated and **(a)** one-hour-ahead, **(b)** three- hour-ahead, **(c)** six-hour-ahead forecasted inundation depths of the O- and R-NARX models during the testing phase at S2.

HESSD
9, 11999–12028, 2012

R-NARX networks for multistep forecasts

H.-Y. Shen and L.-C. Chang

Title Page
Abstract | Introduction
Conclusions | References
Tables | Figures
Back | Close
Full Screen / Esc
Printer-friendly Version
Interactive Discussion

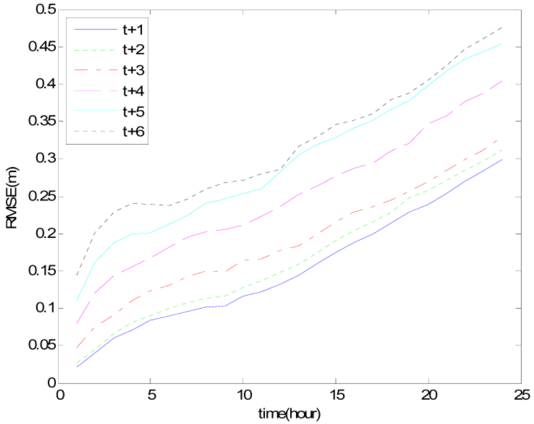

(a) O-NARX

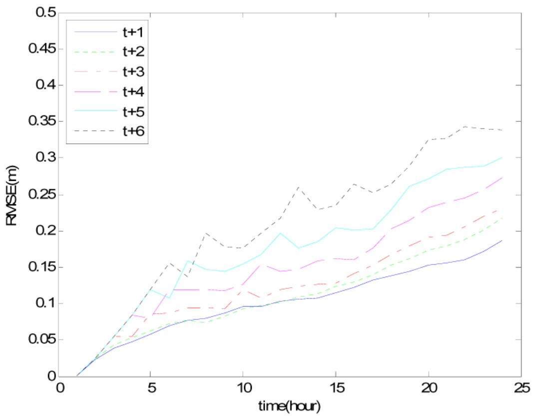

(b) R-NARX

Fig. 8. Stability comparison of the O- and R-NARX modes during the forecast period of 24 h (the mean RMSE of all sites).

HESSD
9, 11999–12028, 2012